

Article

Crystal Contact Engineering for Enhanced Cross-Linking Efficiency of HheG Crystals

Marcel Staar¹, Sophie Staar¹ and Anett Schallmeyer^{1,2,3,*} 

¹ Institute for Biochemistry, Biotechnology and Bioinformatics, Technische Universität Braunschweig, Spielmannstr. 7, 38106 Braunschweig, Germany

² Center of Pharmaceutical Engineering (PVZ), Technische Universität Braunschweig, Franz-Liszt-Str. 35a, 38106 Braunschweig, Germany

³ Braunschweig Integrated Center of Systems Biology (BRICS), Technische Universität Braunschweig, Rebenring 56, 38106 Braunschweig, Germany

* Correspondence: a.schallmeyer@tu-braunschweig.de; Tel.: +49-531-391-55410

Abstract: The generation of cross-linked enzyme crystals is a very attractive method for immobilization of enzymes displaying high crystalizability. However, the commonly used cross-linker glutaraldehyde is not always compatible with enzyme activity. Therefore, we previously reported the engineering of halohydrin dehalogenase HheG from *Ilumatobacter coccineus* to enable thiol-specific cross-linking during CLEC generation by insertion of cysteine residues in the crystal contact. To broaden the applicability of this approach, herein crystal contact engineering of HheG has been performed to incorporate additional lysine residues as defined cross-linking sites for CLEC generation. Using the primary amine-specific cross-linker dithiobis(succinimidyl propionate) (DSP), CLECs of HheG variant V46K were obtained that displayed a high gain in thermal stability compared to wild-type HheG, while using only a low cross-linker concentration. Moreover, respective V46K CLECs exhibited a 10 K higher reaction temperature optimum as well as significantly improved activity and stability at acidic pH and in the presence of organic co-solvents. Overall, our study demonstrates that lysine-specific cross-linkers can also be used as an alternative to glutaraldehyde for stable CLEC generation of halohydrin dehalogenases, and that cross-linking efficiency is significantly improved upon crystal contact engineering.

Keywords: cross-linked enzyme crystals; halohydrin dehalogenase; enzyme immobilization; biocatalysis; enzyme stability



Citation: Staar, M.; Staar, S.; Schallmeyer, A. Crystal Contact Engineering for Enhanced Cross-Linking Efficiency of HheG Crystals. *Catalysts* **2022**, *12*, 1553. <https://doi.org/10.3390/catal12121553>

Academic Editors: Yihan Liu and Liang Zhang

Received: 24 October 2022

Accepted: 29 November 2022

Published: 1 December 2022

Publisher's Note: MDPI stays neutral with regard to jurisdictional claims in published maps and institutional affiliations.



Copyright: © 2022 by the authors. Licensee MDPI, Basel, Switzerland. This article is an open access article distributed under the terms and conditions of the Creative Commons Attribution (CC BY) license (<https://creativecommons.org/licenses/by/4.0/>).

1. Introduction

Enzyme immobilization is a widely used method to stabilize enzymes for application and to enable their reuse as biocatalysts. Carrier-free immobilization in the form of cross-linked enzyme crystals (CLECs) or cross-linked enzyme aggregates (CLEAs) offers the advantage of a high activity-to-volume ratio of the final immobilisate, as no additional carrier is required [1], and has been reported for various types of enzymes such as alcohol dehydrogenases, proteases, lipases or peroxidases [2–8]. Examples of CLEC application in plug-flow reactors or on microfluidic chips have been noted in the literature as well [9–11]. While in the case of CLEC generation the enzyme is crystallized first before cross-linking, CLEAs are obtained after cross-linking of physical enzyme aggregates, resulting in differing mechanical properties of the immobilisate [12]. In both cases, however, glutaraldehyde is the most commonly used cross-linker to introduce covalent chemical links between individual enzyme molecules [13]. As a dialdehyde, glutaraldehyde reacts with amino groups of lysine and arginine side chains of the enzyme, but also with tyrosine to a minor extent [14]. Moreover, as glutaraldehyde is able to form oligomers of different lengths in aqueous solution, residues of various distances are cross-linked with each other, making the use of this cross-linker somewhat unpredictable [14]. Moreover, glutaraldehyde is a

strong irritant, which is toxic to humans and the environment and can even impact enzyme activity in a negative fashion [8,15–17].

Apart from glutaraldehyde, a variety of homo- and heterobifunctional cross-linkers with different specificities are commercially available and can, in principle, be used for CLEC and CLEA generation [18]. In this regard, selective cross-linkers with chemical reactivity towards either primary amines [19,20], thiols [21], or carboxyl-groups [22] are known. Additionally, unselective cross-linkers that can react with various functional groups upon photoactivation have been reported [23]. Moreover, available cross-linkers differ in their solubility as well as cleavability by various agents [18]. In literature, the use of the primary amine-specific cross-linker bis(sulfosuccinimidyl)suberate has been reported for CLEC generation of the lipase from *Burkholderia cepacia* [24]. Likewise, a mix of three different lysine-specific cross-linkers (disuccinimidyl tartrate, dimethyl pimelimidate and ethylene glycol bis(sulfosuccinimidyl) succinate) has been applied to obtain stable CLECs of the halohydrin dehalogenase HheG from *Ilumatobacter coccineus* [25]. Moreover, CLEAs of the lipase from *Penicillium notatum* have also been generated employing a cross-linker that is selective for primary amines [26].

Halohydrin dehalogenases (HHDHs) are lyases, belonging to the superfamily of short-chain dehydrogenases/reductases (SDR), which catalyze the reversible dehalogenation of vicinal haloalcohols resulting in epoxide formation [27]. The reverse reaction, i.e., epoxide ring opening via nucleophilic attack, is of special interest as HHDHs accept a range of different anionic nucleophiles resulting in the formation of new C–C, C–O, C–N and C–S bonds [28]. This has made them useful biocatalysts for the preparation of, e.g., enantioenriched oxazolidinones, tertiary alcohols, epihalohydrines as well as spiroepoxides [29–35]. G-type HHDHs, such as the halohydrin dehalogenase HheG from *I. coccineus*, exhibit a broader substrate scope than other HHDHs as they also display activity towards sterically more demanding cyclic and acyclic non-terminal epoxides [36–38]. This ability to accept also bulky substrates is explained by a much broader active site, as revealed by the crystal structure of HheG [36], in comparison to other structurally characterized HHDHs. As a limitation for industrial application, however, HheG displays a rather low thermal stability with an apparent melting temperature (T_m) of only 38 °C [39]. Protein engineering of HheG with amino acid exchanges at position T123 yielded variants that displayed up to 14 K higher T_m values, as well as improvements in specific activity [39]. Alternatively, carrier-free immobilization of HheG as cross-linked enzyme crystals has been attempted as well. Thus, obtained HheG CLECs cross-linked with glutaraldehyde displayed good mechanical stability but also a strong reduction in enzymatic activity [8,40]. To circumvent the use of glutaraldehyde as cross-linker, protein engineering was applied to incorporate cysteine residues in crystal contacts as new cross-linking sites for thiol-specific cross-linking. Resulting HheG CLECs displayed high stability towards temperature, acidic pH as well as organic co-solvents [8]. To demonstrate the more general validity of our approach to produce active HHDH CLECs, we herein focused on the generation of HheG CLECs cross-linked with alternative primary amine-specific cross-linkers. Thus, crystal contact engineering was applied to design variants carrying additional lysine residues in crystal contacts, resulting in more efficient lysine-specific cross-linking.

2. Results and Discussion

2.1. Crystal Contact Engineering

Although lysines are the least preferred residues in protein crystal contacts [41,42], four lysines are already present in the crystal contact of wild-type HheG crystals with distances of ϵ -amino groups ranging between 9.5 and 17.6 Å (Table S1). Though many lysine-specific cross-linkers with various linker lengths are commercially available [43], lysine-specific cross-linking of wild-type HheG crystals for stable CLEC generation required either high concentrations of a single cross-linker (*vide infra*) or a cross-linker mix to cover the whole range of distances between naturally occurring lysine residues [25]. Alternatively,

the incorporation of additional lysines in the crystal interface by protein engineering was expected to assist in lysine-specific cross-linking using only a single cross-linker.

Our previously described method for crystal contact engineering considered only residues facing each other in the crystal interface within a cut-off distance of 5 Å [8]. As repulsion of positively charged lysines in close proximity could interfere with crystallization, a different approach was taken herein [44]. Previously, Abdul Wahab et al. reported the engineering of surface-exposed residues of the xylanase from *Aspergillus fumigatus* RT-1 to introduce additional lysine residues for generation of CLEAs using glutaraldehyde as cross-linker [45]. The authors used the surface accessibility tool from the Swiss PDB Viewer [46] in order to identify surface-exposed residues for mutagenesis. This strategy was herein adapted for crystal contact engineering of HheG with the addition that possible surface-exposed residues had to be located in the crystal contact as well. Relative surface accessibility (RSA) with a cut-off value of 40% was used to identify surface-exposed residues T44, V46, D53, T78, E89, D115, A141, R185, R208, E214 and D232 in HheG. The location of those residues in the crystal contact of wild-type HheG crystals was checked using the PDBePISA webserver [47]. This analysis revealed that positions D53, E89, R208 and D232 were not located in the crystal contact. Moreover, position E214 forms an ionic interaction with K205 in the tangential crystal contact and was therefore not selected for mutagenesis. As a replacement, residue A217 was used instead as it showed around position E214 the shortest distance between C α atoms to the same residue of the neighboring HheG tetramer in the crystal contact (Figure 1), and still exhibited a reasonably high RSA of >25% (highest value of residues in the crystal contact around E214). In contrast, positions T44 and T78 were rejected because of their too large distance between the same residues of neighboring tetramers. Overall, five different residues of HheG were selected for replacement by lysines: V46 and D115 in the axial crystal contact, as well as A141, R185 and A217 in the tangential crystal contact (Figure 1).

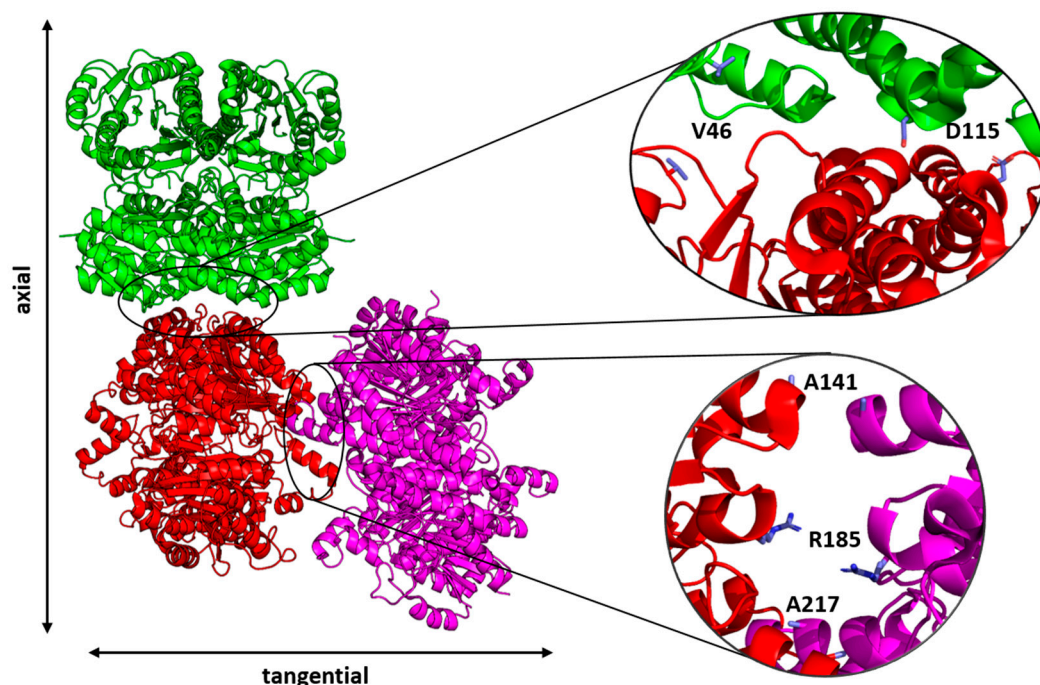


Figure 1. Crystal contact analysis of wild-type HheG (PDB ID: 5O30). Highlighted residues V46 and D115 in the axial crystal contact as well as residues A141, R185 and A217 in the tangential crystal contact were selected for mutagenesis.

Corresponding lysine single mutants V46K, D115K, A141K, R185K and A217K of HheG were generated, heterologously produced in *E. coli* BL21(DE3) with N-terminal His₆-tag and purified via immobilized metal affinity chromatography (IMAC). Respective yields

of purified HheG variants in comparison to wild type are given in Table 1. Additionally, specific activities and obtained product enantiomeric excesses (ee_p) in the azidolysis of cyclohexene oxide (Scheme S1), as well as apparent melting temperatures (T_m) of all variants were determined (Table 1).

Table 1. Specific activities and product enantiomeric excess (ee_p) in the conversion of cyclohexene oxide with azide as nucleophile, as well as apparent melting temperatures (T_m) of HheG wild type and respective variants applied as soluble enzymes. Specific activity and product enantiomeric excess (ee_p) were determined based on duplicate measurements, apparent melting temperatures (T_m) were obtained from triplicate measurements.

Variant	Yield ^[a] [mg/L]	Specific Activity ^[b] [U/mg]	T _m [°C]	ee _p ^[c] [%]
WT	204	2.32 ± 0.3	41	49.1 ± 0.1
V46K	103	0.95 ± 0.02	39	67.8 ± 0.3
D115K	192	1.73 ± 0.01	41	51.5 ± 0.1
A141K	82.8	2.52 ± 0.01	42.5	48.7 ± 0.1
R185K	197	2.26 ± 0.2	42.5	48.9 ± 0.2
A217K	301	2.39 ± 0.01	44	48.3 ± 0.1

^[a] Yield of purified protein per liter of expression culture. ^[b] Reaction conditions: 20 mM cyclohexene oxide, 40 mM sodium azide, 50 µg enzyme in 1.5 mL Tris·SO₄, pH 7.0 at 22 °C and 900 rpm. ^[c] Formation of product enantiomer (1*S*,2*S*)-2-azido-1-cyclohexanol is preferred in all cases.

All variants except V46K exhibited similar specific activities as wild-type HheG in the epoxide ring opening of cyclohexene oxide. In the case of HheG V46K, activity was reduced to 40% of wild type activity. At the same time, the product enantiomeric excess for formation of (1*S*,2*S*)-2-azido-1-cyclohexanol by this variant increased to 68%, compared to only 49% ee_p for wild-type HheG. Thus, HheG V46K is less active but more selective than HheG wild type, which was previously observed for HheG variant M45C as well [8]. In contrast, ee_p values obtained with the other HheG variants were very similar to the wild type value. Moreover, apparent melting temperatures of HheG variants were hardly affected by the introduced amino acid exchanges. All variants were studied further regarding their crystallization properties.

2.2. Crystallization

To find optimal crystallization conditions for the different HheG variants, a crystallization screening was performed as described previously [8]. Variants V46K, A141K and R185K crystallized with even enhanced crystallizability rate and required less time compared to wild-type HheG (Table S2). In contrast, no suitable crystallization conditions could be identified for variants D115K (only precipitate formation) and A217K (no crystal formation, no precipitation). Like wild type, HheG variants V46K, A141K and R185K formed hexagonal-shaped crystals (Figure S1).

Crystallization of these variants was further scaled up to 2 mL scale requiring a change in the crystallization mode from vapor-diffusion to batch crystallization. As a result, no crystals could be obtained for variant R185K in batch mode, while for HheG V46K and A141K the crystallization still worked well using the optimal crystallization conditions identified for vapor-diffusion crystallization. Further optimization of crystallization conditions for HheG R185K in batch mode was not performed, but it is possible that a simple change in, e.g., precipitant or protein concentration could enable R185K crystallization in batch as well [48]. The crystallization kinetics of HheG wild type and its variants in 2 mL batch mode, as shown in Figure 2, can be described by the Avrami equation (Equation (S1) in the supporting information) for crystallization under isothermal conditions [49]. From this, kinetic parameters for crystallization such as the velocity constant (k), the maximal obtainable amount of crystals (S_{max}), the Avrami exponent (n) and the half time of the crystallization process (t_{0.5}) could be determined (Table S3). For comparison, the previously described cysteine variant HheG D114C, which

has been generated earlier for thiol-specific cross-linking of HheG during CLEC formation [8], was included in this analysis as well. As indicated already in Figure 2 and in agreement with previous results [8], HheG variants D114C [$k = 0.249 \text{ h}^{-1}$] and A141K [$k = 0.133 \text{ h}^{-1}$] crystallized faster than wild type [$k = 0.011 \text{ h}^{-1}$], and also reached higher yields of crystallized protein (0.69 and $0.63 \text{ mg}_{\text{crystal}}/\text{mg}_{\text{protein}}$ for D114C and A141K, respectively, compared to $0.55 \text{ mg}_{\text{crystal}}/\text{mg}_{\text{protein}}$ for wild-type HheG after 72 h of crystallization). This is also in agreement with the observed higher crystallizability of those variants compared to wild type under vapor-diffusion conditions. In contrast, variant V46K showed opposite behavior with a lower k of only 0.003 h^{-1} and a lower yield of crystallized protein ($0.47 \text{ mg}_{\text{crystal}}/\text{mg}_{\text{protein}}$) under the used crystallization conditions in batch mode. This reduced crystallization efficiency of HheG V46K in batch, compared to vapor-diffusion crystallization, could likely be improved again by optimization of respective crystallization conditions.

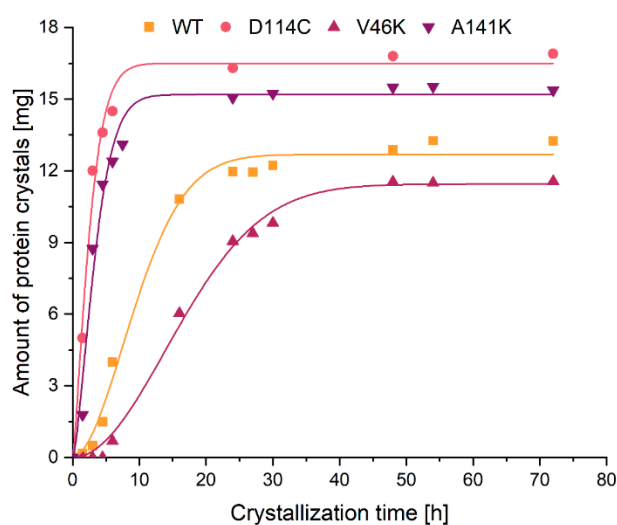


Figure 2. Avrami-based crystallization kinetics of different HheG variants. Crystallization was performed with gentle shaking at 8°C . A total amount of 24 mg protein was used for crystallization.

Regarding the Avrami exponent n , which describes the crystallization behavior and is defined by Equation (S2) [50], the obtained values for all studied variants range between 1.3 and 2.0. Those values are in agreement with the theoretically expected range of 1.5 to 2.5 for a 3-dimensional, diffusion-controlled protein crystal growth [51]. As the Avrami exponent is dependent on the nucleation rate, observed differences in the crystallization kinetics of the different HheG variants are probably caused by differences in nucleation. Thus, variants with smaller Avrami exponent (D114C, A141K) likely exhibited a faster nucleation rate, whereas variants with higher Avrami exponent (wild type, V46K) probably displayed a slower nucleation rate.

2.3. Cross-Linking

After investigations into the crystallization behavior, HheG wild type as well as variants V46K and A141K were cross-linked using different lysine-specific cross-linkers of varying spacer length, including disuccinimidyl tartrate (DST, 6.4 Å spacer length), dimethyl pimelimidate (DMP, 9.2 Å spacer length), dimethyl suberimidate (DMS, 11 Å spacer length), dithiobis(succinimidyl) propionate (DSP, 12 Å spacer length) and ethylene glycol bis(sulfosuccinimidyl) succinate (Sulfo-EGS, 16.1 Å spacer length) (Table S4). Cross-linkers were used in concentrations of 4, 10, 20 and 40 mM. The efficiency of cross-linking was evaluated in terms of CLEC stability after cross-linking using the thermal shift assay. This approach is based on our earlier findings that effective cross-linking results in an increase in apparent melting temperature (T_m) of formed CLECs [8]. Exemplary melting curves of wild-type HheG and variant V46K in soluble and CLEC form are shown in

Figure S2 in the supplementary. Resulting T_m values of the CLECs obtained after cross-linking of HheG wild type and variants V46K and A141K with different lysine-specific cross-linkers are illustrated in Figure 3.

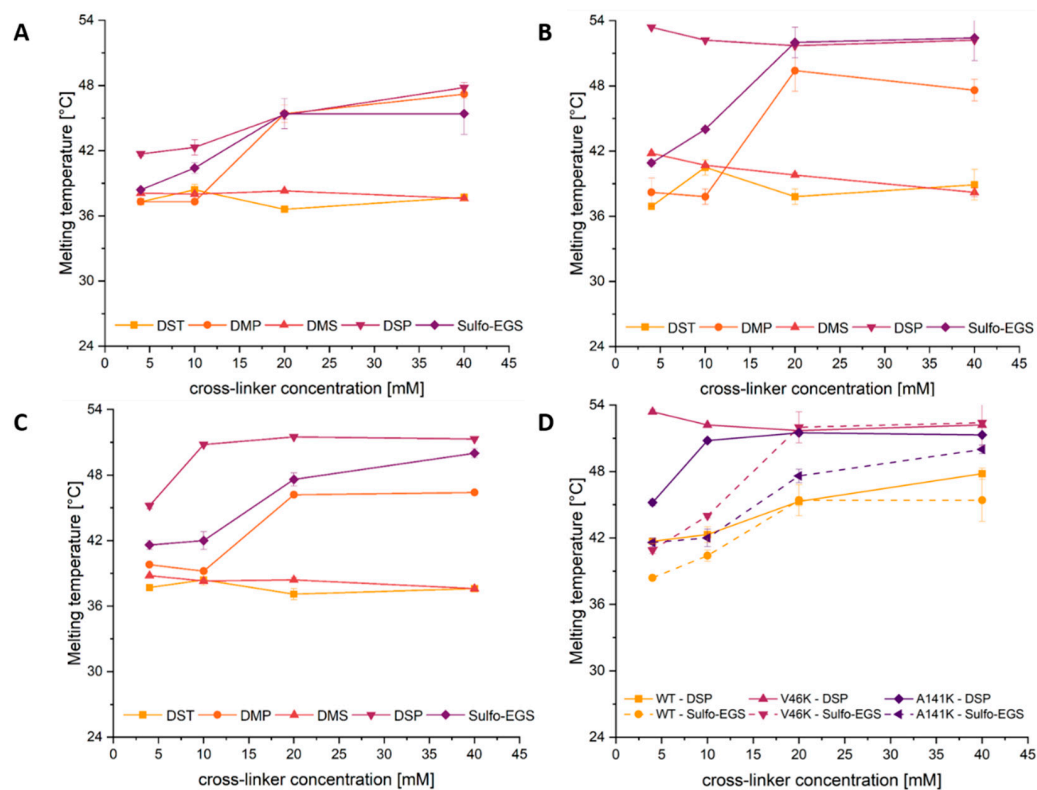


Figure 3. Influence of the concentration of different cross-linkers on CLEC stability. Apparent melting temperatures of CLECs of wild-type HheG (A) as well as variants V46K (B) and A141K (C) were determined after cross-linking with five different cross-linkers and using increasing cross-linker concentrations. (D) Comparison of the different CLEC variants cross-linked with either DSP or Sulfo-EGS. Melting temperatures were determined in triplicate.

As mentioned before, wild-type HheG harbors four lysines in the crystal interface. Thus, it can already be cross-linked by lysine-specific cross-linkers DMP, DSP and Sulfo-EGS—as determined by an increase in apparent melting temperature—without insertion of additional lysines in the crystal contact (Figure 3A). However, high cross-linker concentrations (≥ 20 mM) are required to achieve this. At a concentration of 20 mM, all three cross-linkers yielded the same gain in thermal stability of resulting CLECs compared to soluble wild-type HheG. In contrast, CLECs of variants with additionally incorporated lysine residues in the crystal contact displayed a significantly stronger gain in stability compared to wild type. V46K CLECs (Figure 3B) reached apparent melting temperatures of 53 °C and 52 °C using cross-linkers DSP and Sulfo-EGS, respectively. Likewise, DSP was also the most efficient cross-linker for variant A141K (Figure 3C). In case of cross-linker DMP, the incorporation of additional lysine residues did not improve CLEC stability further compared to HheG wild type. In contrast, cross-linkers DMS and DST did not yield any gain in stability among all variants, which is likely due to insufficient cross-linking. A comparison of all three HheG variants (wild type, V46K and A141K) with cross-linkers DSP and Sulfo-EGS (Figure 3D) revealed that the incorporation of additional lysine residues in the crystal contact not only improves CLEC stability compared to wild type, but also enables the use of lower cross-linker concentrations for efficient cross-linking. While 20 mM DSP are required for efficient cross-linking of wild type CLECs, 10 mM or 4 mM DSP are sufficient for stable cross-linking of variants A141K and V46K, respectively. The observed differences in cross-linking efficiency can be explained by the actual distance

of lysine residues in the crystal interface of individual variants as well as the chemical characteristics of the used cross-linker. Thus, cross-linker DST with a spacer length of only 6.4 Å seems to be too short for effective cross-linking of any HheG variant. Moreover, DMS and DMP are imidoester-type cross-linkers and have been reported to be less stable (half-life ≤ 30 min [52]) than N-hydroxysuccinimid (NHS)-type cross-linkers (half-life of 4–5 h [53]) such as DSP, DST and Sulfo-EGS [18]. Additionally, NHS-type cross-linkers achieve effective cross-linking under physiological conditions (pH 7.0–7.4), while optimum pH values for cross-linking with imidoesters range between pH 8.5 and 9.0 [18,19,53]. Since in this study, cross-linking has been performed in buffers with pH ranging from pH 7.0–7.5 (Table S2), NHS-type cross-linkers DSP and Sulfo-EGS are expected to cross-link more effectively than imidoester-type cross-linkers DMS and DMP. The higher efficiency of DSP compared to Sulfo-EGS might be explained by different linker lengths (12 Å and 16.1 Å, respectively). Thus, DSP might fit more ideally between two interfacial lysines for cross-linking than Sulfo-EGS. On the other hand, there might be a stronger diffusional limitation for the larger cross-linker Sulfo-EGS within the HheG crystal [54] compared to DSP, resulting in a less effective cross-linking of enzyme molecules in the crystal interior.

A more detailed cross-linking study of V46K CLECs using cross-linker DSP further revealed that 1 h cross-linking time is sufficient to obtain highly stable CLECs ($T_m = 53$ °C) at a DSP concentration of 4 mM, while lower cross-linker concentrations (<4 mM DSP) yield CLECs with lower increase in apparent melting temperature compared to soluble enzyme (Figure S3).

2.4. CLEC Activity

In addition to stability, the biocatalytic activity of the generated CLECs in comparison to soluble enzyme was also investigated. For this, all three HheG variants (wild type, A141K and V46K) were individually cross-linked with the cross-linkers DMP, DSP and Sulfo-EGS, which resulted in an improvement of CLEC stability upon cross-linking. Cross-linker concentrations were selected based on Figure 3 to achieve high CLEC stability in each case. Thus, DMP and Sulfo-EGS were used in concentrations of 20 mM for all variants. In the case of DSP, the cross-linker concentration was adjusted individually depending on the HheG variant (20 mM for wild type, 10 mM for variant A141K and 4 mM for variant V46K). Resulting conversions in the ring opening of cyclohexene oxide with azide after 24 h using 100 µg of biocatalyst are summarized in Figure 4. This revealed that the cross-linker DMP had a significant negative effect on CLEC activity for all three HheG variants, as the conversion achieved with those CLECs was only in the range of the negative control reaction without enzyme. A similar negative trend was also observed for variants V46K and A141K with Sulfo-EGS, while wild type CLECs cross-linked with the same cross-linker still yielded 67% conversion (compared to 90% for soluble wild-type HheG). The applied high concentration of both cross-linkers (20 mM for each variant) might explain this observed dramatic reduction in enzymatic activity. It has previously been reported that high concentrations of the cross-linker glutaraldehyde can result in reduced enzyme activity, probably based on partial inactivation of the enzyme [17]. Moreover, when using the lysine-specific, NHS-type cross-linker bis(sulfosuccinimidyl)suberate to generate CLECs of the lipase from *Burkholderia cepacia*, a decrease in enzymatic activity was observed at higher cross-linker concentration [24]. The negative effect of high (≥ 10 mM) concentrations of cross-linker DSP on CLEC activity of HheG wild type and A141K was less pronounced, but still significant. In contrast, V46K CLECs not only displayed the highest conversion among all tested CLECs, but also yielded an improved product enantiomeric excess (62.9%) compared to soluble wild type (48.8%). The high CLEC activity is probably explained by the lower required cross-linker concentration. Thus, HheG variant V46K cross-linked with DSP was investigated further.

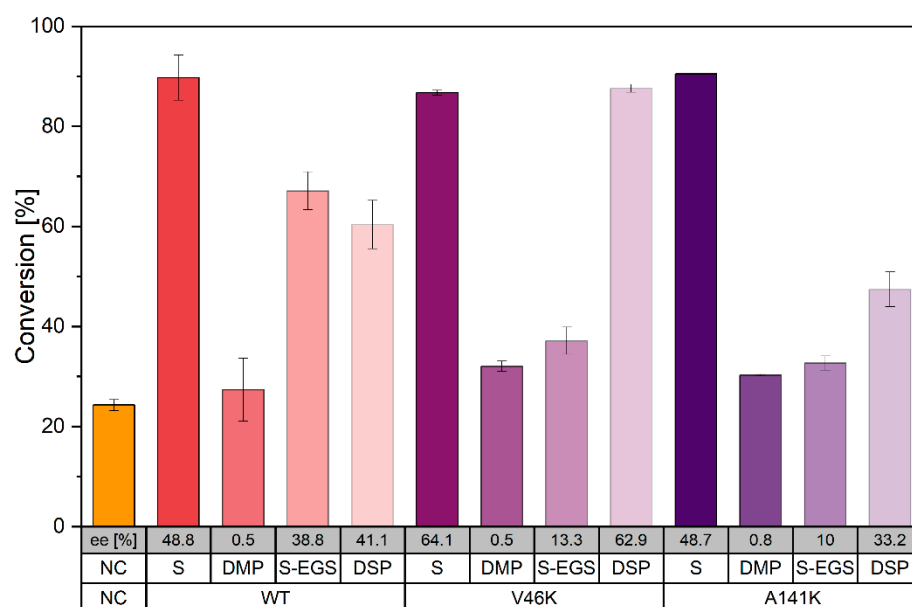


Figure 4. Conversion and product enantiomeric excess obtained in reactions of 20 mM cyclohexene oxide with 40 mM azide using 100 μg biocatalyst (soluble or CLECs) after 24 h. A 20 mM cross-linker concentration was used during cross-linking with DMP and Sulfo-EGS. In case of DSP, 4 mM, 10 mM or 20 mM cross-linker concentration was applied for cross-linking of HheG variants V46K, A141K and wild type, respectively. Measurements were performed in quintuplicates. ‘NC’ indicates negative control and ‘S’ soluble enzyme. The product enantiomeric excess (ee) obtained in the negative control reaction was 0.5%.

2.5. Further CLEC Characterization

As the crystal size plays a crucial role for CLEC activity, a particle size distribution analysis of V46K CLECs was performed. The resulting sum (Figure S4A) and density distributions (Figure S4B) revealed that most CLECs exhibited a particle size of around 2 μm . Additionally, some CLECs displayed a larger particle size of 5–70 μm . For comparison, the same result was obtained for CLECs of HheG variant D114C (Figure S3). Since the median value of particle size for the V46K CLECs ($d_{50} = 2.17 \mu\text{m}$, Table S5) is below 10 μm , it can be assumed that there are no diffusional limitations during catalysis [55].

The observed higher apparent melting temperature of V46K CLECs compared to its soluble form was further confirmed by a 14 K higher T_{50} value (referring to the temperature at which 50% of the enzyme activity is retained after incubation for 30 min) (Figure S5), as well as a 10 K higher optimal reaction temperature (35 $^{\circ}\text{C}$ for V46K CLECs compared to 25 $^{\circ}\text{C}$ for soluble enzyme) (Figure 5A). Moreover, V46K CLECs still displayed activity up to 45 $^{\circ}\text{C}$, while soluble HheG V46K was fully inactivated already at 30 $^{\circ}\text{C}$.

Likewise, the pH profile of V46K CLECs was broadened with higher activity at acidic pH values compared to soluble enzyme (Figure 5B). This phenomenon was also observed in previous work for CLECs of HheG D114C [8]. Based on the catalytic mechanism of HHDHs, the catalytic Tyr165 donates a proton to the negatively charged oxygen during epoxide ring opening, and re-protonation of this tyrosine is facilitated at acidic pH [27]. This also explains the shift in the pH optimum of V46K CLECs to pH 5, at which soluble enzyme is already inactive. The increased stability of V46K CLECs at acidic pH was also demonstrated by thermal shift assay revealing significantly higher T_m values of the CLECs at acidic conditions compared to soluble enzyme (Figure S6).

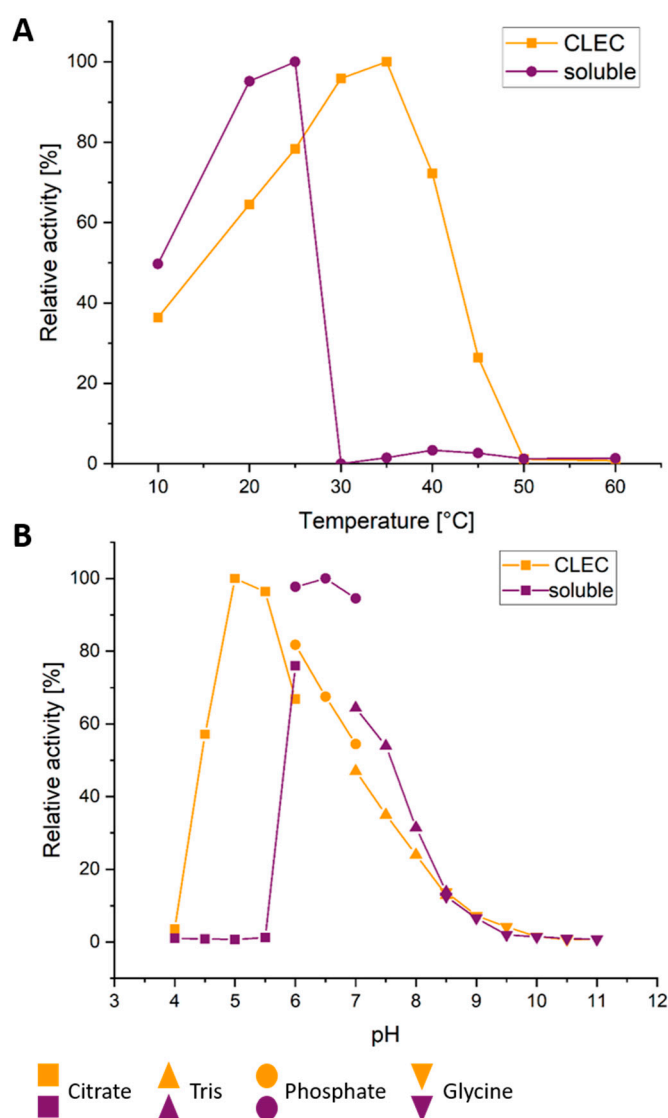


Figure 5. Temperature (A) and pH (B) profile of V46K CLECs and soluble enzyme in epoxide ring opening of 20 mM cyclohexene oxide with 40 mM azide and 100 μ g biocatalyst. Reactions were performed for 2 h in duplicates, and the highest conversion was set to 100% relative activity. The 100% relative activity corresponds to 42.5% (soluble) and 44.5% (CLEC) absolute conversion for (A), and 65.1% (soluble) and 65.3% (CLEC) for (B).

Organic solvents play a major role in industrial applications as they allow to solubilize higher amounts of substrates [56]. In previous work, a low tolerance of HheG wild type towards water-miscible organic solvents has been shown [39], while the previously reported CLECs of HheG variant D114C still displayed significant activity in the presence of organic co-solvents [8]. Hence, the tolerance of V46K CLECs towards such co-solvents was also investigated. In contrast to soluble HheG V46K, the CLECs were still significantly active in the presence of 25% (*v/v*) dimethylformamide, isopropanol, ethanol and methanol (Figure 6). In the case of 25% (*v/v*) dimethylsulfoxide, soluble HheG V46K still displayed some residual activity, while respective CLECs were significantly more active. Only 25% (*v/v*) acetonitrile resulted in full inactivation of soluble enzyme and the CLECs, which has been described previously for HheG D114C as well [8]. Additionally, apparent melting temperatures of HheG V46K in soluble and CLEC form were determined in the presence of 10% (*v/v*) organic solvent (Table S6). The results indicate that DMSO has the lowest destabilizing effect on both enzyme preparations, which is consistent with corresponding activity data in the presence of this co-solvent. The tested alcohols methanol, ethanol

and isopropanol had the same destabilizing effect on the CLECs as on soluble HheG V46K, whereas the reduction in T_m was significantly lower for the CLECs compared to soluble enzyme when using 10% (*v/v*) acetonitrile or dimethylformamide. Interestingly, the reduction in T_m of the CLECs caused by acetonitrile was lower compared to the reduction in T_m caused by isopropanol, even though the CLECs proved still active in the presence of the latter co-solvent but inactive with acetonitrile. This could indicate that acetonitrile may exert an additional inhibitory effect on the enzyme preparations, as reported for the co-solvent DMSO in combination with the halohydrin dehalogenase HheC from *Agrobacterium radiobacter* AD1 [57].

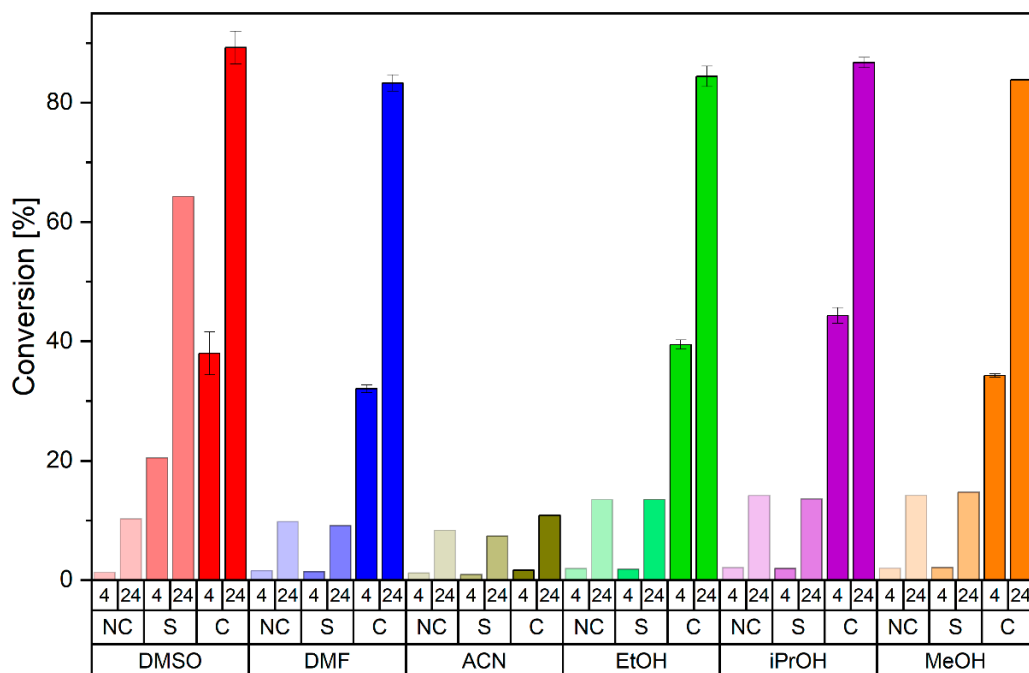


Figure 6. Conversion of 20 mM cyclohexene oxide and 40 mM azide in the presence of 25% (*v/v*) water-miscible organic solvents using either 100 μ g V46K CLECs or soluble enzyme. Investigated solvents were dimethyl sulfoxide (DMSO), dimethyl formamide (DMF), acetonitrile (ACN), ethanol (EtOH), isopropanol (iPrOH) and methanol (MeOH). Samples were taken after 4 and 24 h. Reactions were performed in duplicates. ‘NC’ indicates negative control without enzyme, ‘S’ soluble enzyme and ‘C’ CLECs.

Finally, enzymatic half-life ($t_{1/2}$) at a reaction temperature of 22 $^{\circ}$ C was determined as described previously [8,58] to evaluate the long-term stability of the generated V46K CLECs. For this, deactivation rate constants k_d for soluble enzyme and CLECs at three different temperatures above 30 $^{\circ}$ C were determined experimentally (Table S7) and respective k_d values at 22 $^{\circ}$ C were extrapolated from the corresponding Eyring plot (Figure S7) using the Eyring equation (Equation (S3)). Based on these deactivation rate constants at 22 $^{\circ}$ C, deactivation energies (E_d) and enzymatic half-life times of HheG V46K in soluble and CLEC form were calculated using Equations (S4) and (S5), respectively (Table S8). Thus, a half-life time of 82 days at 22 $^{\circ}$ C was obtained for V46K CLECs, while the $t_{1/2}$ value for the soluble enzyme was only 23 h. This result is comparable to the previously reported half-life time of HheG D114C CLECs (64 days) in comparison to soluble enzyme (21 h) [8]. Likewise, the calculated deactivation energy of the CLECs (47.5 kJ/mol) is significantly increased compared to soluble HheG V46K (36.5 kJ/mol). The observed increases in half-life and deactivation energy upon immobilization are also consistent with other literature reports [17,59].

As reported previously for CLECs of HheG variant D114C cross-linked with BMOE [8], reuse of HheG V46K CLECs in repetitive batch reactions of cyclohexene oxide with azide

over 21 cycles could be demonstrated as well (Figure S8). In the case of V46K CLECs, however, a significant drop in conversion after the first reaction cycle, down to 54% conversion in the fourth cycle, was observed in all five parallel measurements. In contrast, conversion decreased only slightly in all subsequent reaction cycles. Hence, we suppose that this significant drop at the beginning is rather caused by a loss of the smallest CLECs during centrifugation and exchange of reaction media, instead of an actual decrease in CLEC activity due to inactivation. In future applications, such a loss could be avoided, e.g., by use of a membrane reactor [60].

3. Materials and Methods

3.1. Chemicals

Substrate cyclohexene oxide as well as cross-linkers DST, DMP, DMS, DSP and Sulfo-EGS (Table S4) were purchased from Thermo Fisher Scientific (Geel, Belgium). All chemicals were of highest available purity.

3.2. Bacterial Strains and Plasmids

E. coli DH5 α was used for cloning and other genetic manipulations whereas *E. coli* BL21(DE3) gold was used for heterologous protein production. Further, expression vector pET-28a(+) (Merck, Darmstadt, Germany) was used to clone respective genes under control of the T7 promoter while adding an N-terminal His₆-tag to heterologously produced proteins.

3.3. HheG Engineering

Amino acid positions of HheG were selected based on their position at the crystal interface as well as their general surface accessibility, which was determined using the surface accessibility tool from the Swiss PDB viewer [46] and the previously reported crystal structure of HheG (PDB: 5O30 [36]). Amino acids with a minimum of 40% relative surface accessibility were selected. Site-directed mutagenesis of HheG was performed using the PfuUltra II Hotstart PCR Mastermix (Agilent Technologies, Santa-Clara, CA, USA). Forward and reverse mutagenic primers (Table 2) were designed with PrimerX (Carlo Lapid, 2003, <http://bioinformatics.org/primerx/index.htm>, accessed on 16 June 2020), purchased from Merck (Darmstadt, Germany) and used in concentrations of 0.25 μ M each with 100 ng of pET28a(+)-*hheG* template [39]. Otherwise, the PCR protocol for mutagenesis was in agreement with the manufacturer's instructions. As the final step, parental (methylated) DNA was digested using 20 U DpnI.

Table 2. Mutagenic primers used in this study. Nucleotide exchanges are shown in bold.

Mutagenic Primer	Sequence 5'–3'
f_hheG_V46K	CAGCCGGTGATGGCACCATGAAAGGTGTTGAAGAAAGTTTTG
r_hheG_V46K	CAAAACTTTCTCAACACCTTTCATGGTGCCATCACCGGCT
f_hheG_D115K	GCAAATTTCTGGATATGACCGATA AAAC AGTGGGCAAAGTTAAAGCAACC
r_hheG_D115K	GGTTGCTTTAACTTTTGCCACTGTTTATCGGTCATATCCAGAAATTTGC
f_hheG_A141K	GTTCTGCCTCCGATGGTTAAAGCCGGTGCAGGTCAGTG
r_hheG_A141K	CACTGACCTGCACCGGCTT TA ACCATCGGAGGCAGAAC
f_hheG_R185K	GCAGTTGGTCTGGAACATGCA AAAC ATGGTGTTCAGGTTAATGC
r_hheG_R185K	GCATTAACCTGAACACCATGTTTTCATGTTCCAGACCAACTGC
f_hheG_A217K	GATGGTGATCCGGAACGTCGTA AAAT GATTGAAGCACAGGTTTC
r_hheG_A217K	GAACCTGTGCTCAATCATT TTT TACGACGTTCCGGATCACCATC

3.4. Protein Production and Purification

Protein production and purification of all HheG variants was performed as previously described for wild-type HheG [8,36]. Protein production was carried out in *E. coli* BL21 (DE3) gold cells at 22 °C for 24 h. After cell disruption by sonication, HheG variants were purified via immobilized metal affinity chromatography (IMAC) making use of the

N-terminal hexahistidine-tag. Desalted protein solutions were stored at $-20\text{ }^{\circ}\text{C}$ until further use.

3.5. Activity and Enantioselectivity Determination

Specific activities of HheG wild type and its variants were determined as described previously [8]. Briefly, reactions of 20 mM cyclohexene oxide with 40 mM sodium azide were investigated in 1.5 mL reaction volumes in 50 mM Tris·SO₄, pH 7.0 at 22 °C (900 rpm in an Eppendorf ThermoMixer C). After starting reactions by addition of 50 µg enzyme, samples were taken after 1, 3, 5, 10, 15, 30, and 60 min and extracted with an equal volume of *tert*-butyl methyl ether (TBME) containing 0.1% (*v/v*) *n*-dodecane. Organic phases were dried over MgSO₄, and samples were analyzed by achiral gas chromatography (GC; see supplementary material for details regarding GC analysis).

Determination of conversion and enantioselectivity of soluble enzymes and CLECs in the azidolysis of 20 mM cyclohexene oxide was performed in 1 mL Tris·SO₄, pH 7.0 using 100 µg biocatalyst and 40 mM sodium azide. Conversion was determined after 4 and 24 h with achiral GC. Product enantiomeric excess was determined after 4 h reaction time using chiral GC. Used temperature programs and resulting retention times of compounds in achiral and chiral GC analyses are listed in Table S9.

3.6. Crystallization and Cross-Linking

Crystallization in 2, 20 and 200 µL scale was performed as described previously [8]. Crystallization in 2 mL scale was performed under gentle shaking in 15 mL tubes (Sarstedt, Nümbrecht, Germany) for 24 h at 8 °C. Crystallization buffers for respective variants (see Table S2) were mixed 1:1 with a 24 mg/mL concentrated protein solution. Crystal formation was analyzed using a SMZ-171-TLED microscope (Moticeurope, Barcelona, Spain). To determine the amount of crystallized protein, samples were centrifuged for 3 min at 400× *g* and the amount of crystallized protein was inferred from the remaining protein absorbance at 280 nm in the supernatant.

Cross-linking of crystals in 20 µL and 200 µL scale was performed as described previously [8]. In 200 µL scale, crystals of HheG wild type as well as variants A141K and V46K were cross-linked with each 4, 10, 20 and 40 mM of cross-linkers DSP, DMP, DST, DMS or Sulfo-EGS (see Table S4) to determine CLEC stability via thermal shift assay. To investigate the effect of cross-linking time and cross-linker concentration on V46K CLEC stability, crystals of HheG V46K were cross-linked for different times (3, 6, 18, 24, 48, 72 h) and with different cross-linker concentrations (0.5, 1, 2, 5, 10, 20), and afterwards analyzed via thermal shift assay.

For cross-linking in 2 mL scale, crystals of HheG V46K were centrifuged for 3 min at 400× *g* after crystallization. The supernatant was discarded and obtained crystals were cross-linked in 2 mL crystallization buffer containing 4 mM DSP. Cross-linking was performed under gentle shaking at 8 °C for 24 h. Afterwards, CLECs were harvested by centrifugation, washed with 2 mL Tris·SO₄, pH 7.0 and centrifuged again. Resulting CLECs were resuspended in Tris·SO₄, pH 7.0 to a concentration of 2 mg/mL. For biocatalytic reactions, each 50 µL (corresponding to 100 µg of CLECs) of this solution were transferred to the reaction mixture by pipetting with a truncated tip.

3.7. Temperature, pH and Solvent Activity Profiles

To determine temperature-dependent activity profiles, reactions of 1 mL were performed under standard reaction conditions (20 mM cyclohexene oxide and 40 mM azide in 50 mM Tris·SO₄, pH 7.0 at 22 °C and 900 rpm) at different temperatures (10, 20, 25, 30, 35, 40, 45, 50, and 60 °C). Samples were taken after 2 h and analyzed via achiral GC. Maximum conversion was set to 100% relative activity. Reactions were performed in duplicate.

To obtain pH-dependent activity profiles, reactions of 1 mL were performed under standard reaction conditions using different buffer systems of varying pH (50 mM citrate buffer at pH 4–6, 50 mM phosphate buffer at pH 6–7, 50 mM Tris·SO₄ buffer at pH 7–8.5 and

glycine·NaOH buffer at pH 8.5–11). Samples were taken after 2 h and analyzed via achiral GC. Maximum conversion was set to 100% relative activity. Reactions were performed in duplicate.

To assess activities in the presence of different organic co-solvents, reactions were performed under standard reaction conditions with 25% (*v/v*) of co-solvents such as ethanol, methanol, isopropanol, acetonitrile, dimethylsulfoxide and dimethylformamide. Sampling of duplicate reactions was performed after 4 and 24 h and analyzed by achiral GC.

3.8. Thermal Shift Assay

Thermal shift assay of soluble enzyme and CLECs to determine apparent melting temperatures (T_m) was performed as described previously [8]. Each measurement contained 10 μ g soluble enzyme or 20 μ g CLECs, 5 \times SYPRO orange fluorescent dye and TE buffer in a total of 50 μ L volume. It should be noted that high residual cross-linker concentrations in the CLEC sample can disturb the measurement, probably due to interference with the SYPRO orange fluorescent dye.

For obtaining melting temperatures in the presence of different co-solvents, thermal shift assays contained 10% (*v/v*) of the following solvents: ethanol, methanol, isopropanol, acetonitrile, dimethylsulfoxide, dimethylformamide. For the determination of melting temperatures at other pH values, TE buffer was replaced by either 50 mM citrate buffer (pH 4–6), 50 mM phosphate buffer (pH 6–7), 50 mM Tris·SO₄ buffer (pH 7–8.5), or glycine·NaOH buffer (pH 8.5–11).

3.9. Thermal Inactivation

T_{50} values of HheG V46K in soluble and CLEC form were determined based on residual activity after incubation at various temperatures. Aliquots of 100 μ g biocatalyst were first incubated for each 30 min at different temperatures (10, 20, 30, 32.9, 35.7, 38.6, 41.4, 44.3, 47.1, 50, 60, or 70 °C). Afterwards, residual activity was determined in the conversion of cyclohexene oxide with azide using standard reaction conditions (20 mM epoxide and 40 mM azide in 50 mM Tris·SO₄, pH 7.0 at 22 °C and 900 rpm for 2 h). Samples were analyzed by achiral GC analysis. T_{50} values were obtained using the Boltzman fit in OriginPro 2021 (OriginLab Corporation, Northampton, MA, USA).

3.10. Determination of Half-Life Times

Half-life times ($t_{1/2}$) of soluble HheG V46K and V46K CLECs at 22 °C were obtained based on the determination of deactivation rate constants (k_d) as described previously [8]. Deactivation rate constants at 30, 32 and 34 °C for soluble enzyme, and 36, 38, 40 °C for CLECs were determined by incubating the enzyme preparations at respective temperatures. After 0, 15, 30, 60, 90, 120, 180 and 240 min of incubation, samples were taken for reactions containing 50 μ g soluble enzyme or 100 μ g CLECs, 20 mM cyclohexene oxide and 40 mM azide at 22 °C and 900 rpm to determine conversions after 30 min. The natural logarithm of conversion was plotted against time, to derive the corresponding deactivation rate constant at a given temperature from the respective slope after linear regression. Using an Eyring plot in combination with the Eyring equation, deactivation rate constants for soluble enzyme and CLECs at 22 °C could be extrapolated, from which corresponding deactivation energies (E_d) and half-life times ($t_{1/2}$) could be calculated as described previously [8].

3.11. Reusability

For the determination of V46K CLEC reusability, consecutive batch reactions were performed in 1 mL as described in Section 3.5 with 100 μ g CLECs. After 24 h, samples were taken for achiral GC analysis (Table S9). Then, the remaining reaction mixture was centrifuged for 3 min at 400 \times g and fresh reaction medium was added. This procedure was repeated for 21 days with daily sampling. Reactions were performed in quintuplicates.

3.12. Particle Size Distribution

Particle size analysis of generated CLECs was performed via laser diffraction using a Mastersizer 3000 (Malvern Panalytical, Kassel, Germany). A 2 mL amount of a concentrated CLEC solution (5.5 mg/mL for V46K CLECs, 8.5 mg/mL for D114C CLECs) was used for wet particle size distribution analysis. Particle size distributions were determined in triplicate and the average was displayed as sum and density distribution as well as 10, 50 and 90% cumulative undersizes (d_{10} , d_{50} , d_{90}) (Table S5).

4. Conclusions

In addition to our previously described example for cross-linking of HheG crystals with a thiol-specific cross-linker, another example has been given herein to demonstrate the applicability of our crystal contact engineering approach for CLEC generation of halohydrin dehalogenases, this time employing lysine-specific cross-linking. Though lysines are naturally occurring in the crystal contact of HheG already, the targeted incorporation of additional lysine residues enabled the use of considerably lower cross-linker concentrations to yield highly stable and active CLECs. Thus, cross-linking efficiency was enhanced significantly through crystal contact engineering.

Apart from that, the best cross-linker for CLEC generation of a given enzyme still has to be identified empirically, as this will depend, on the one hand, on the distance of amino acid side chains to be cross-linked and the actual cross-linking conditions. On the other hand, this will be affected as well by the impact of the individual cross-linker and the respective cross-linking site on enzyme activity of the formed CLECs. In our example, the lysine-specific cross-linker DSP proved best for generation of highly stable CLECs of all three HheG variants, wild type as well as mutants V46K and A141K, but its impact on CLEC activity varied significantly.

Resulting V46K CLECs cross-linked with DSP displayed significantly higher stability regarding temperature, pH and co-solvent concentrations compared to the soluble enzyme, as previously described for HheG D114C CLECs cross-linked with BMOE [8]. This confirms that CLEC generation after crystal contact engineering is a highly useful method to obtain robust HheG preparations for application, which will prove valuable for immobilization of further HHDHs and other enzymes with high crystallizability as well.

Supplementary Materials: The following supporting information can be downloaded at: <https://www.mdpi.com/article/10.3390/catal12121553/s1>, Scheme S1. Epoxide ring opening of cyclohexene oxide (1) catalyzed by HheG wild type and its variants using azide as nucleophile [2a: (1R,2R)-2-azido-1-cyclohexanol, 2b: (1S,2S)-2-azido-1-cyclohexanol]; Table S1. Distances of natural lysines as well as residues selected for mutagenesis within the crystal contact of wild type HheG; Table S2. Crystallization characteristics of different HheG variants based on crystallization in 2 μ L scale; Figure S1. Hexagonal-shaped crystals of HheG wild type (A) and variants V46K (B), A141K (C), and R185K (D) after 72 h of crystallization.; Table S3. Crystallization kinetic parameters of different HheG variants based on the theory of Avrami of isothermal phase change; Table S4. Structure and spacer length of the lysine-specific cross-linkers DST, DMP, DMS, DSP and Sulfo-EGS used in this study; Figure S2. First derivative of the measured fluorescence signal obtained by thermal shift analysis of wild-type HheG (A) and variant V46K (B) in soluble and CLEC form.; Figure S3. Dependency of apparent melting temperature (T_m) of HheG V46K CLECs (cross-linked with DSP) on cross-linker concentration and cross-linking time; Figure S4. Particle size distribution analysis; Table S5. Cumulative undersizes for 10, 50 and 90% of D114C and V46K CLECs; Figure S5. Thermal inactivation of HheG V46K in soluble and CLEC form; Figure S6. Melting temperature (T_m) determination of HheG V46K in soluble and CLEC form depending on pH; Table S6. Difference in apparent melting temperature (ΔT_m) of soluble HheG V46K and V46K CLECs in the presence and absence of 10% (v/v) co-solvent; Table S7. Experimentally determined deactivation rate constants (k_d) at the respective temperatures for HheG V46K CLECs and soluble enzyme; Figure S7. Eyring plot of deactivation rate constants determined for HheG V46K in soluble and CLEC form; Table S8. Half-life time ($t_{1/2}$) and deactivation energy (E_d) of HheG V46K CLECs and soluble enzyme at 22 °C; Figure S8. Repetitive batch reactions of

cyclohexene oxide and azide at 22 °C with reuse of HheG V46K CLECs.; Table S9. GC temperature programs and retention times of substrates and products used in this study [39,49,50,58].

Author Contributions: Conceptualization, A.S.; Data curation, M.S.; Formal analysis, M.S.; Funding acquisition, A.S.; Investigation, M.S. and S.S.; Methodology, M.S.; Project administration, A.S.; Resources, A.S.; Supervision, A.S.; Validation, M.S. and A.S.; Visualization, M.S.; Writing—original draft, M.S.; Writing—review and editing, S.S. and A.S. All authors have read and agreed to the published version of the manuscript.

Funding: This research was funded by the German Research Foundation (DFG) within the Priority Programme 1934 (DiSPBiotech), grant number SCHA 1745/2-2. The APC was funded through the same project.

Data Availability Statement: The data that support the findings of this study are either contained in the Supplementary Information or are available from the corresponding author upon reasonable request.

Acknowledgments: Technical support by Marta Kubiak (Institute for Particle Technology and Center of Pharmaceutical Engineering, Technische Universität Braunschweig) regarding particle size distribution analysis is gratefully acknowledged.

Conflicts of Interest: The authors declare no conflict of interest.

References

1. Cao, L.; van Langen, L.; Sheldon, R.A. Immobilised Enzymes: Carrier-Bound or Carrier-Free? *Curr. Opin. Biotechnol.* **2003**, *14*, 387–394. [[CrossRef](#)]
2. Liao, Q.; Du, X.; Jiang, W.; Tong, Y.; Zhao, Z.; Fang, R.; Feng, J.; Tang, L. Cross-Linked Enzyme Aggregates (CLEAs) of Halohydrin Dehalogenase from *Agrobacterium radiobacter* AD1: Preparation, Characterization and Application as a Biocatalyst. *J. Biotechnol.* **2018**, *272–273*, 48–55. [[CrossRef](#)] [[PubMed](#)]
3. Clair, N.S.; Wang, Y.-F.; Margolin, A.L. Cofactor-Bound Cross-Linked Enzyme Crystals (CLEC) of Alcohol Dehydrogenase. *Angew. Chem. Int. Ed.* **2000**, *39*, 380–383. [[CrossRef](#)]
4. Persichetti, R.A.; Clair, N.L.S.; Griffith, J.P.; Navia, M.A.; Margolin, A.L. Cross-Linked Enzyme Crystals (CLECs) of Thermolysin in the Synthesis of Peptides. *J. Am. Chem. Soc.* **1995**, *117*, 2732–2737. [[CrossRef](#)]
5. Noritomi, H.; Koyama, K.; Kato, S.; Nagahama, K. Increased Thermostability of Cross-Linked Enzyme Crystals of Subtilisin in Organic Solvents. *Biotechnol. Tech.* **1998**, *12*, 467–469. [[CrossRef](#)]
6. Ayala, M.; Horjales, E.; Pickard, M.A.; Vazquez-Duhalt, R. Cross-Linked Crystals of Chloroperoxidase. *Biochem. Biophys. Res. Commun.* **2002**, *295*, 828–831. [[CrossRef](#)]
7. Lalonde, J.J.; Govardhan, C.; Khalaf, N.; Martinez, A.G.; Visuri, K.; Margolin, A.L. Cross-Linked Crystals of *Candida rugosa* Lipase: Highly Efficient Catalysts for the Resolution of Chiral Esters. *J. Am. Chem. Soc.* **1995**, *117*, 6845–6852. [[CrossRef](#)]
8. Staar, M.; Henke, S.; Blankenfeldt, W.; Schallmey, A. Biocatalytically Active and Stable Cross-Linked Enzyme Crystals of Halohydrin Dehalogenase HheG by Protein Engineering. *ChemCatChem* **2022**, *14*, e202200145. [[CrossRef](#)]
9. Roy, J.J.; Abraham, T.E. Continuous Biotransformation of Pyrogallol to Purpurogallin Using Cross-Linked Enzyme Crystals of Laccase as Catalyst in a Packed-Bed Reactor. *J. Chem. Technol. Biotechnol.* **2006**, *81*, 1836–1839. [[CrossRef](#)]
10. Fernández-Penas, R.; Verdugo-Escamilla, C.; Martínez-Rodríguez, S.; Gavira, J.A. Production of Cross-Linked Lipase Crystals at a Preparative Scale. *Cryst. Growth Des.* **2021**, *21*, 1698–1707. [[CrossRef](#)]
11. Conejero-Muriel, M.; Rodríguez-Ruiz, I.; Martínez-Rodríguez, S.; Llobera, A.; Gavira, J.A. McCLEC, a Robust and Stable Enzymatic Based Microreactor Platform. *Lab Chip* **2015**, *15*, 4083–4089. [[CrossRef](#)] [[PubMed](#)]
12. Cui, J.D.; Jia, S.R. Optimization Protocols and Improved Strategies of Cross-Linked Enzyme Aggregates Technology: Current Development and Future Challenges. *Crit. Rev. Biotechnol.* **2015**, *35*, 15–28. [[CrossRef](#)] [[PubMed](#)]
13. Jegan Roy, J.; Emilia Abraham, T. Strategies in Making Cross-Linked Enzyme Crystals. *Chem. Rev.* **2004**, *104*, 3705–3722. [[CrossRef](#)] [[PubMed](#)]
14. Migneault, I.; Dartiguenave, C.; Bertrand, M.J.; Waldron, K.C. Glutaraldehyde: Behavior in Aqueous Solution, Reaction with Proteins, and Application to Enzyme Crosslinking. *BioTechniques* **2004**, *37*, 790–802. [[CrossRef](#)] [[PubMed](#)]
15. Takigawa, T.; Endo, Y. Effects of Glutaraldehyde Exposure on Human Health. *J. Occup. Health* **2006**, *48*, 75–87. [[CrossRef](#)]
16. Leung, H.-W. Ecotoxicology of Glutaraldehyde: Review of Environmental Fate and Effects Studies. *Ecotoxicol. Environ. Saf.* **2001**, *49*, 26–39. [[CrossRef](#)]
17. Roy, J.J.; Abraham, T.E. Preparation and Characterization of Cross-Linked Enzyme Crystals of Laccase. *J. Mol. Catal. B Enzym.* **2006**, *38*, 31–36. [[CrossRef](#)]
18. Mattson, G.; Conklin, E.; Desai, S.; Nielander, G.; Savage, M.D.; Morgensen, S. A Practical Approach to Crosslinking. *Mol. Biol. Rep.* **1993**, *17*, 167–183. [[CrossRef](#)]

19. Staros, J.V. N-Hydroxysulfosuccinimide Active Esters: Bis(N-Hydroxysulfosuccinimide) Esters of Two Dicarboxylic Acids Are Hydrophilic, Membrane-Impermeant, Protein Cross-Linkers. *Biochemistry* **1982**, *21*, 3950–3955. [[CrossRef](#)]
20. Staros, J.V. Membrane-Impermeant Crosslinking Reagents: Probes of the Structure and Dynamics of Membrane Proteins. *Acc. Chem. Res.* **1988**, *21*, 435–441. [[CrossRef](#)]
21. Auclair, J.R.; Boggio, K.J.; Petsko, G.A.; Ringe, D.; Agar, J.N. Strategies for Stabilizing Superoxide Dismutase (SOD1), the Protein Destabilized in the Most Common Form of Familial Amyotrophic Lateral Sclerosis. *Proc. Natl. Acad. Sci. USA* **2010**, *107*, 21394–21399. [[CrossRef](#)] [[PubMed](#)]
22. Grabarek, Z.; Gergely, J. Zero-Length Crosslinking Procedure with the Use of Active Esters. *Anal. Biochem.* **1990**, *185*, 131–135. [[CrossRef](#)]
23. Brinkley, M. A Brief Survey of Methods for Preparing Protein Conjugates with Dyes, Haptens and Crosslinking Reagents. *Bioconjugate Chem.* **1992**, *3*, 2–13. [[CrossRef](#)] [[PubMed](#)]
24. Hetrick, E.M.; Sperry, D.C.; Nguyen, H.K.; Strege, M.A. Characterization of a Novel Cross-Linked Lipase: Impact of Cross-Linking on Solubility and Release from Drug Product. *Mol. Pharm.* **2014**, *11*, 1189–1200. [[CrossRef](#)]
25. Kubiak, M.; Kampen, I.; Schilde, C. Structure-Based Modeling of the Mechanical Behavior of Cross-Linked Enzyme Crystals. *Crystals* **2022**, *12*, 441. [[CrossRef](#)]
26. Rehman, S.; Bhatti, H.N.; Bilal, M.; Asgher, M. Cross-Linked Enzyme Aggregates (CLEAs) of *Penicillium notatum* Lipase Enzyme with Improved Activity, Stability and Reusability Characteristics. *Int. J. Biol. Macromol.* **2016**, *91*, 1161–1169. [[CrossRef](#)]
27. Schallmey, A.; Schallmey, M. Recent Advances on Halohydrin Dehalogenases—From Enzyme Identification to Novel Biocatalytic Applications. *Appl. Microbiol. Biotechnol.* **2016**, *100*, 7827–7839. [[CrossRef](#)] [[PubMed](#)]
28. Hasnaoui-Dijoux, G.; Majerić Elenkov, M.; Spelberg, J.H.L.; Hauer, B.; Janssen, D.B. Catalytic Promiscuity of Halohydrin Dehalogenase and Its Application in Enantioselective Epoxide Ring Opening. *ChemBioChem* **2008**, *9*, 1048–1051. [[CrossRef](#)]
29. Wan, N.; Tian, J.; Zhou, X.; Wang, H.; Cui, B.; Han, W.; Chen, Y. Regioselective Ring-Opening of Styrene Oxide Derivatives Using Halohydrin Dehalogenase for Synthesis of 4-Aryloxazolidinones. *Adv. Synth. Catal.* **2019**, *361*, 4651–4655. [[CrossRef](#)]
30. Majerić Elenkov, M.; Tang, L.; Meetsma, A.; Hauer, B.; Janssen, D.B. Formation of Enantiopure 5-Substituted Oxazolidinones through Enzyme-Catalysed Kinetic Resolution of Epoxides. *Org. Lett.* **2008**, *10*, 2417–2420. [[CrossRef](#)]
31. Majerić Elenkov, M.; Hoeffken, H.W.; Tang, L.; Hauer, B.; Janssen, D.B. Enzyme-Catalyzed Nucleophilic Ring Opening of Epoxides for the Preparation of Enantiopure Tertiary Alcohols. *Adv. Synth. Catal.* **2007**, *349*, 2279–2285. [[CrossRef](#)]
32. Lutje Spelberg, J.H.; van Hylckama Vlieg, J.E.T.; Bosma, T.; Kellogg, R.M.; Janssen, D.B. A Tandem Enzyme Reaction to Produce Optically Active Halohydrins, Epoxides and Diols. *Tetrahedron Asymmetry* **1999**, *10*, 2863–2870. [[CrossRef](#)]
33. Majerić Elenkov, M.; Primožič, I.; Hrenar, T.; Smolko, A.; Dokli, I.; Salopek-Sondi, B.; Tang, L. Catalytic Activity of Halohydrin Dehalogenases towards Spiroepoxides. *Org. Biomol. Chem.* **2012**, *10*, 5063–5072. [[CrossRef](#)] [[PubMed](#)]
34. Zhang, F.-R.; Wan, N.-W.; Ma, J.-M.; Cui, B.-D.; Han, W.-Y.; Chen, Y.-Z. Enzymatic Kinetic Resolution of Bulky Spiro-Epoxyoxindoles via Halohydrin Dehalogenase-Catalyzed Enantio- and Regioselective Azidolysis. *ACS Catal.* **2021**, *11*, 9066–9072. [[CrossRef](#)]
35. Xu, Q.; Huang, K.-S.; Wang, Y.-F.; Wang, H.-H.; Cui, B.-D.; Han, W.-Y.; Chen, Y.-Z.; Wan, N.-W. Stereodivergent Synthesis of Epoxides and Oxazolidinones via the Halohydrin Dehalogenase-Catalyzed Desymmetrization Strategy. *ACS Catal.* **2022**, *12*, 6285–6293. [[CrossRef](#)]
36. Koopmeiners, J.; Diederich, C.; Solarczek, J.; Voß, H.; Mayer, J.; Blankenfeldt, W.; Schallmey, A. HheG, a Halohydrin Dehalogenase with Activity on Cyclic Epoxides. *ACS Catal.* **2017**, *7*, 6877–6886. [[CrossRef](#)]
37. Calderini, E.; Wessel, J.; Süß, P.; Schrepfer, P.; Wardenga, R.; Schallmey, A. Selective Ring-Opening of Di-Substituted Epoxides Catalysed by Halohydrin Dehalogenases. *ChemCatChem* **2019**, *11*, 2099–2106. [[CrossRef](#)]
38. Solarczek, J.; Kaspar, F.; Bauer, P.; Schallmey, A. G-Type Halohydrin Dehalogenases Catalyze Ring Opening Reactions of Cyclic Epoxides with Diverse Anionic Nucleophiles. *Chem. Eur. J.* **2022**, e202202343. [[CrossRef](#)]
39. Solarczek, J.; Klünemann, T.; Brandt, F.; Schrepfer, P.; Wolter, M.; Jacob, C.R.; Blankenfeldt, W.; Schallmey, A. Position 123 of Halohydrin Dehalogenase HheG Plays an Important Role in Stability, Activity, and Enantioselectivity. *Sci. Rep.* **2019**, *9*, 5106. [[CrossRef](#)]
40. Kubiak, M.; Staar, M.; Kampen, I.; Schallmey, A.; Schilde, C. The Depth-Dependent Mechanical Behavior of Anisotropic Native and Cross-Linked HheG Enzyme Crystals. *Crystals* **2021**, *11*, 718. [[CrossRef](#)]
41. Dasgupta, S.; Iyer, G.H.; Bryant, S.H.; Lawrence, C.E.; Bell, J.A. Extent and Nature of Contacts between Protein Molecules in Crystal Lattices and between Subunits of Protein Oligomers. *Proteins* **1997**, *28*, 494–514. [[CrossRef](#)]
42. Iyer, G.H.; Dasgupta, S.; Bell, J.A. Ionic Strength and Intermolecular Contacts in Protein Crystals. *J. Cryst. Growth* **2000**, *217*, 429–440. [[CrossRef](#)]
43. Han, K.-K.; Richard, C.; Delacourte, A. Chemical Cross-Links of Proteins by Using Bifunctional Reagents. *Int. J. Biochem.* **1984**, *16*, 129–145. [[CrossRef](#)]
44. Derewenda, Z.S. Rational Protein Crystallization by Mutational Surface Engineering. *Structure* **2004**, *12*, 529–535. [[CrossRef](#)]
45. Abdul Wahab, M.K.H.; El-Enshasy, H.A.; Bakar, F.D.A.; Murad, A.M.A.; Jahim, J.M.; Illias, R.M. Improvement of Cross-Linking and Stability on Cross-Linked Enzyme Aggregate (CLEA)-Xylanase by Protein Surface Engineering. *Process Biochem.* **2019**, *86*, 40–49. [[CrossRef](#)]

46. Guex, N.; Peitsch, M.C. SWISS-MODEL and the Swiss-Pdb Viewer: An Environment for Comparative Protein Modeling. *Electrophoresis* **1997**, *18*, 2714–2723. [[CrossRef](#)] [[PubMed](#)]
47. Krissinel, E.; Henrick, K. Inference of Macromolecular Assemblies from Crystalline State. *J. Mol. Biol.* **2007**, *372*, 774–797. [[CrossRef](#)] [[PubMed](#)]
48. Chayen, N.E. Comparative Studies of Protein Crystallization by Vapour-Diffusion and Microbatch Techniques. *Acta Cryst. D* **1998**, *54*, 8–15. [[CrossRef](#)]
49. Avrami, M. Kinetics of Phase Change. I General Theory. *J. Chem. Phys.* **1939**, *7*, 1103–1112. [[CrossRef](#)]
50. Moreno-Cencerrado, A.; Iturri, J.; Toca-Herrera, J.L. In-Situ 2D Bacterial Crystal Growth as a Function of Protein Concentration: An Atomic Force Microscopy Study. *Microsc. Res. Tech.* **2018**, *81*, 1095–1104. [[CrossRef](#)]
51. Khayati, G.R.; Nourafkan, E.; Karimi, G.; Moradgholi, J. Synthesis of Cuprous Oxide Nanoparticles by Mechanochemical Oxidation of Copper in High Planetary Energy Ball Mill. *Adv. Powder Technol.* **2013**, *24*, 301–305. [[CrossRef](#)]
52. Sinz, A. Chemical Cross-Linking and Mass Spectrometry for Mapping Three-Dimensional Structures of Proteins and Protein Complexes. *J. Mass Spectrom.* **2003**, *38*, 1225–1237. [[CrossRef](#)]
53. Lomant, A.J.; Fairbanks, G. Chemical Probes of Extended Biological Structures: Synthesis and Properties of the Cleavable Protein Cross-Linking Reagent [³⁵S]Dithiobis(Succinimidyl Propionate). *J. Mol. Biol.* **1976**, *104*, 243–261. [[CrossRef](#)] [[PubMed](#)]
54. Margolin, A.L.; Navia, M.A. Protein Crystals as Novel Catalytic Materials. *Angew. Chem. Int. Ed.* **2001**, *40*, 2204–2222. [[CrossRef](#)]
55. Kasvinsky, P.J.; Madsen, N.B. Activity of Glycogen Phosphorylase in the Crystalline State. *J. Biol. Chem.* **1976**, *251*, 6852–6859. [[CrossRef](#)] [[PubMed](#)]
56. Cseri, L.; Razali, M.; Pogany, P.; Szekeley, G. Chapter 3.15—Organic Solvents in Sustainable Synthesis and Engineering. In *Green Chemistry*; Török, B., Dransfield, T., Eds.; Elsevier: Amsterdam, The Netherlands, 2018; pp. 513–553. ISBN 978-0-12-809270-5.
57. Milčić, N.; Štepanić, V.; Crnolatac, I.; Findrik Blažević, Z.; Brkljača, Z.; Majerić Elenkov, M. Inhibitory Effect of DMSO on Halohydrin Dehalogenase: Experimental and Computational Insights into the Influence of an Organic Co-Solvent on the Structural and Catalytic Properties of a Biocatalyst. *Chem. Eur. J.* **2022**, *28*, e202201923. [[CrossRef](#)]
58. Eyring, H.; Stearn, A.E. The Application of the Theory of Absolute Reaction Rates to Proteins. *Chem. Rev.* **1939**, *24*, 253–270. [[CrossRef](#)]
59. Maurya, S.S.; Nadar, S.S.; Rathod, V.K. A Rapid Self-Assembled Hybrid Bio-Microflowers of Alpha-Amylase with Enhanced Activity. *J. Biotechnol.* **2020**, *317*, 27–33. [[CrossRef](#)]
60. Taboada-Puig, R.; Junghanns, C.; Demarche, P.; Moreira, M.T.; Feijoo, G.; Lema, J.M.; Agathos, S.N. Combined Cross-Linked Enzyme Aggregates from Versatile Peroxidase and Glucose Oxidase: Production, Partial Characterization and Application for the Elimination of Endocrine Disruptors. *Bioresour. Technol.* **2011**, *102*, 6593–6599. [[CrossRef](#)] [[PubMed](#)]